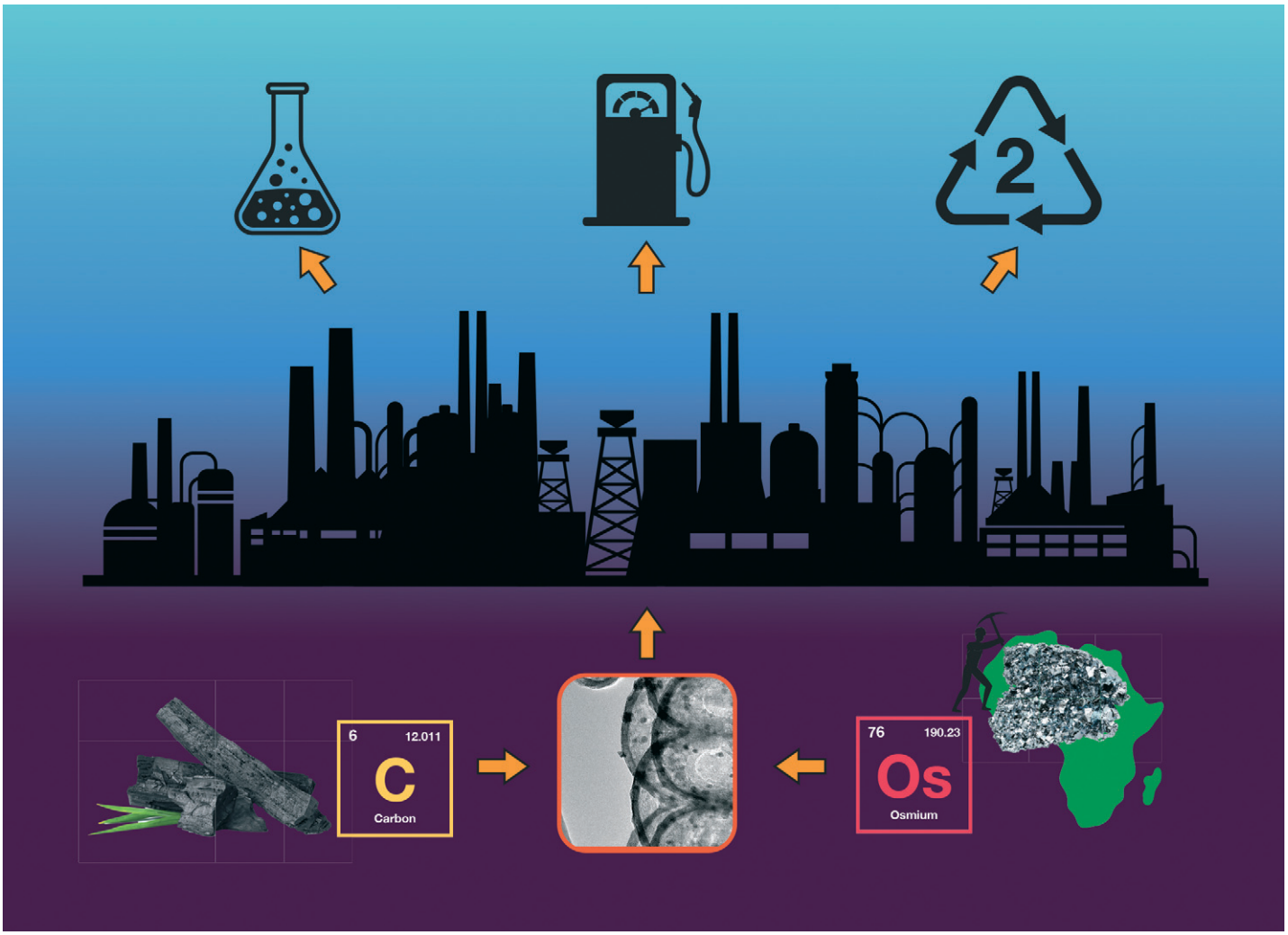

Showcasing research from Professor Coville's laboratory, School of Chemistry, University of the Witwatersrand, Johannesburg, South Africa.

The effect of separation distance on hydrogen spillover in Os promoted Co@HCS catalysts

The distance over which hydrogen can travel in a spillover effect on a hollow sphere (HCS) carbon support has been evaluated using temperature reduction profiles. In this study, Os/(Co@HCSx) and Co@HCSx (x = HCS shell thickness; 16 nm, 28 nm, 51 nm) catalysts were studied and hydrogen spillover for the reduction of the Co by the Os was found to vary with HCS thickness and Co oxidation state.

As featured in:

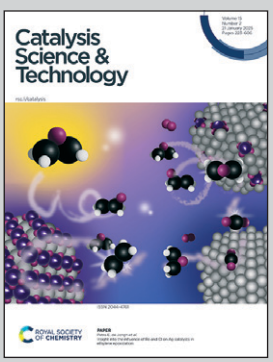

See Neil John Coville *et al.*, *Catal. Sci. Technol.*, 2025, **15**, 334.

ROYAL SOCIETY OF CHEMISTRY

rsc.li/catalysis

Registered charity number: 207890

Catalysis Science & Technology

ROYAL SOCIETY OF CHEMISTRY

PAPER

View Article Online
View Journal | View Issue

Cite this: *Catal. Sci. Technol.*, 2025, **15**, 334

The effect of separation distance on hydrogen spillover in Os promoted Co@HCS catalysts†

Tshepo Molefe, [abc] Roy Peter Forbes [ab] and Neil John Coville *[ab]

Spillover effects from an easily reduced metal (Os) to a less easily reduced metal (Co) were investigated by use of hollow carbon spheres (HCSs) of different shell thicknesses, *x*, (*x* = 16 nm, 28 nm and 51 nm). The Co (10%) was loaded inside the HCS and the Os (1%) outside three HCS supports (Os/Co@HCS*x*). Temperature programmed reduction, together with BET and XRD studies, were used to monitor the effects of the Os on the Co as a function of HCS shell thickness. When no Os was present on the outside of the HCSs, the effect of H_2 diffusion on the two Co reduction peaks was determined. Comparison with the Os containing Co@HCSs catalysts indicated that the two Co reduction peaks were influenced differently by the HCS shell thickness. Spillover of hydrogen could be observed at distances of *ca.* >100 nm, as shown by the shift of the first Co reduction peak (Co_3O_4 to CoO) while that of the second reduction peak (CoO to Co) was only observed at distances up to *ca.* 50 nm. The disordered carbon material is proposed to be responsible for the H transfer reaction between Os and Co. The Os/(Co@HCS*x*) catalysts were tested for Fischer–Tropsch (FT) activity and the data indicated a drop in the FT activity with shell thickness. This suggests that HCSs require an optimum thickness (to provide stability, good porosity and auto-reduction behaviour) to generate high FT activity/selectivity, with spillover effects aiding the reaction.

Received 18th June 2024,
Accepted 27th September 2024

DOI: 10.1039/d4cy00758a

rsc.li/catalysis

1. Introduction

Hydrogen spillover is an important mechanism that involves the transfer of hydrogen from an easily reduced atom per s to a more difficult to reduce atom per s.[1] The process is important in both catalysis and in hydrogen storage.[2] In catalysis, hydrogen transfer allows for a metal oxide to be reduced by H atoms that are transferred from a reduced metal atom to the metal oxide, which is an easier energy process than the direct reduction of the metal oxide by hydrogen molecules.

This process of H transfer to the metal oxide is dependent on many factors such as i) the metal species that is reduced by H_2 (Fig. 1, metal a), ii) the metal oxide to be reduced (Fig. 1, metal b), iii) the material (support) that separates the metals, a and b and iv) the distance between metals a and b denoted by *x*.

When the metals are in close contact (referred to as a primary spillover process)[3–6] the transfer of H atoms is straightforward and is viewed as a classical promoter effect, an important step in many catalytic reactions. When the two metal components are separated, a process called secondary spillover can occur.[7–13] The material (support) that separates the two components has been shown to be affected by the support reducibility and by defects in the support.[2] The classic separation material to observe the secondary spillover effect is TiO_2; this arises since TiO_2 can easily be reduced.[8] Other supports that have been studied include alumina, tungsten, and various carbons. The study of these support materials has been extensively explored as the supports have been implicated for use in hydrogen storage *via* spillover effects.[2,14]

An issue that has been less explored is that of the separation distance between the two metals *i.e.* the distance (*x*) between metal a and b in Fig. 1. Various methods have been used to study this issue. These include i) the synthesis of the two metals (or oxides) on separate supports followed by a separation of the two materials by additional support material,[15–18] ii) deposition of the two metals on a substrate

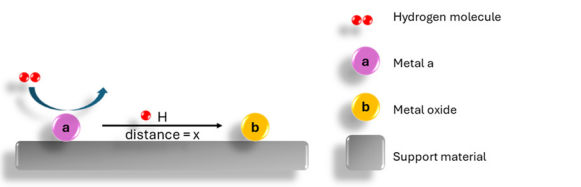

Fig. 1 Schematic diagram for the H atom transfer (hydrogen spillover effect).

[a] *DSI-NRF Centre of Excellence in Catalysis (c*change), South Africa*
[b] *The Molecular Sciences Institute, School of Chemistry, University of the Witwatersrand, Johannesburg 2050, South Africa. E-mail: neil.coville@wits.ac.za*
[c] *Institute for Catalysis and Energy Solutions (ICES), College of Science, Engineering and Technology, University of South Africa (UNISA), Private Bag X6 Florida 1710, Johannesburg, South Africa*

† Electronic supplementary information (ESI) available. See DOI: https://doi.org/10.1039/d4cy00758a

separated by known distances[8,19] and iii) the use of chemical barriers to separate the two materials[20,21] (Fig. 2).

Studies to date have focused on metal oxide supports to study the separation process. Indeed, the excellent study by Karim *et al.* has revealed the different behaviour of TiO_2 and Al_2O_3 as separation media for the study of Fe catalysts reduced by spillover from Pt.[8] Many carbons with different morphologies have also been used as the support to study spillover effects. Carbon support materials with oxygen groups on their surface are thought to improve the metal–carbon interaction and to allow better active metal dispersion and thus to enhance the spillover effect. These include activated carbon,[3–6] carbon nanofibers,[22–24] carbon nanotubes,[25–32] fullerenes,[33] carbon nanospheres,[34] graphene-like materials,[35–39] and templated carbon[35,40–42] and all have been the subject of experimental studies on hydrogen spillover with carbon materials. However, while the effect of carbon as a separation media has been explored no studies have been reported on the effect of carbon separation distance on spillover. Indeed, very few studies have been carried out to study the effect of distance on any support.[2,43,44]

A type of carbon that has been used as a support material is the hollow carbon sphere (HCS). This has a spherical hollow structure, and the inside can be used as a nanoreactor, by encapsulating an active metal phase within the carbon shell. These metal–HCS materials have been used in different catalytic reactions such as oxidation, nitroarene reduction, hydrogenation, Fischer–Tropsch synthesis (FTS), and the integration of multiple catalytic reactions.[45–50]

Herein we report on a model system in which hollow carbon spheres (HCSs) with adjustable diameter was used to separate an easily reduced metal (Os) from a cobalt catalyst, for use in Fischer–Tropsch Synthesis reactions (Fig. 3, $d_1 < d_2$) in order to study distance spillover effects. The shells were made porous to enable H_2 diffusion. The choice of this model system is related to our earlier study where it was shown that Os (like other easily reduced metals such as Pt and Ru) could readily be separated from Co by the carbon shell in a HCS and act as a promoter for cobalt.[21]

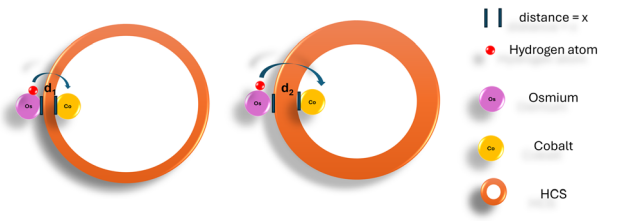

Fig. 3 Schematic diagram of HCS with different shell thickness ($d_1 < d_2$) for studying the hydrogen spillover effect between Os and Co.

2. Experimental

2.1 Materials and methods

All reagents used for the syntheses described here were of analytical grade and were purchased from various chemical suppliers. All reagents used in these syntheses were used as received. This includes the following chemical reagents: cobalt nitrate hexahydrate ($Co(NO_3)_2{\cdot}6H_2O$) (Aldrich), potassium osmate ($K_2[OsO_2(OH)_2]$) (Anglo American Research Laboratories, Johannesburg), ammonia solution (25%; Fluka), ethanol (98%; Merck), hexadecyltrimethylammonium bromide ($C_{19}H_{42}BrN$) (CTAB; Aldrich), styrene (Aldrich), polyvinylpyrrolidone ($(C_6H_9NO)_n$) (PVP, MW 40 K, Aldrich) formaldehyde (37%; Aldrich), potassium persulfate ($K_2S_2O_8$) (Eimer and Amend), hydrazine (35% Aldrich), and deionized water. All reagents were used as received. The polystyrene spheres (PSSs) used in the study were all synthesized by a published procedure.[51]

2.2 Synthesis of Co@HCS catalyst

2.2.1 Synthesis of 10%Co loaded on PSS (Co/PSS). PSSs (3 g)[51] were dispersed in a mixture of 75 mL deionized water and 25 ml ethanol. To this mixture was added cobalt nitrate hexahydrate (0.45 g), while stirring, until the solution turned

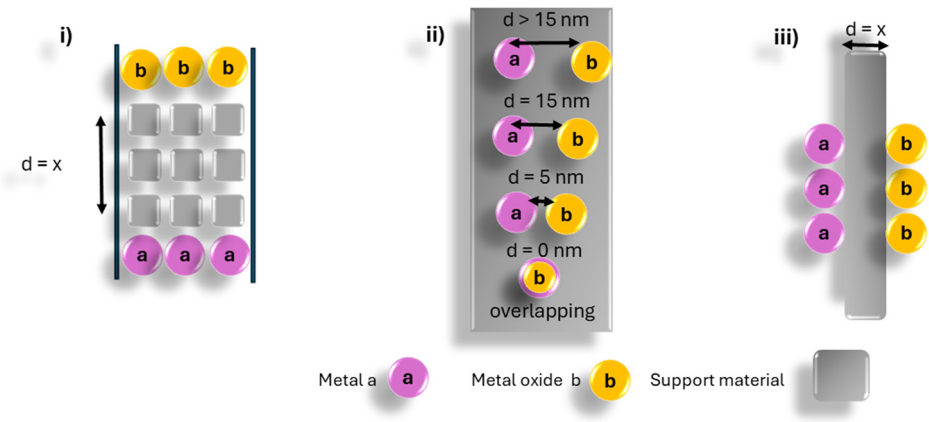

Fig. 2 Schematic diagram of a metal (a) and a metal oxide (b) to be reduced by a spillover effect when i) they are on separate supports with the two support materials 1 and 2 being separated by an inert support material, ii) on a substrate separated by known distances (*x*), iii) separated by a chemical barrier (support material).

red. Thereafter, 10 mL of hydrazine (2 M) was slowly added to the prepared solution dropwise and the solution was then stirred for 12 h to ensure complete deposition of Co nanoparticles onto the PSSs to give Co/PSSs.[21] Yields of >90% were obtained.

2.2.2 Synthesis of Co@HCS with different shell thickness. The Co/PSSs (Co = 10%) (3 g) in ammonia solution (25%; 12 mL) were dispersed in a mixture of 150 mL ethanol and 76 ml deionized water by sonication for 30 min. Subsequently, resorcinol (1.1 g), formaldehyde (2.3 mL) and hexadecyltrimethylammonium bromide (2.5 g) were added to make the resorcinol–formaldehyde core–shell structure. The solution was allowed to stir at room temperature for 24 h. The formed Co/PSSs–resorcinol–formaldehyde (RF) core–shell structure was filtered and washed successively with water and ethanol, followed by drying at 80 °C for 12 h. Template removal and carbonization of the prepared composites was performed in a two-step horizontal chemical vapour deposition apparatus. The template removal was done under a flow of nitrogen gas (50 ml min^{-1}) at 350 °C for 1 h to decompose the PSSs. This was followed by the carbonization of the RF core–shell structure under a flow of nitrogen gas (50 ml min^{-1}) at 600 °C for 2 h to give the Co@HCS.[52]

The synthesis parameters used to tune the HCS shell, was done by varying the reactant ratios (Table 1). The different Co@HCS materials were made with three different shell thicknesses of 16 ± 3 nm, 28 ± 5 nm, and 51 ± 6 nm and are referred to as Co@HCS16, Co@HCS28, Co@HCS51 respectively.

2.2.3 Synthesis of 1%Os loaded on Co@HCS with different diameters. The Co@HCS*x* (*x* = 16, 28, 51) (1.5 g) catalysts were dispersed in 250 mL of deionized water by sonication. This mixture was added to the Os salt precursor (0.069 g, Os = 1%, 1 : 32 Os : Co molar ratio) and urea (0.4 g) followed by 30 min sonication. The mixture was then stirred at 95 °C in a round bottom flask for 12 h. The product Os/(Co@HCS) was collected after filtration and washing with water, followed by drying at 80 °C for 12 h. Yields of >90% were obtained.

2.3 Characterization techniques and Fischer–Tropsch synthesis catalyst evaluation

All characterization techniques used, and FT catalyst evaluation data are reported in the ESI† section (Section S1.1 and S1.3, respectively). The standard procedures/conditions can also be found in an earlier publication.[21]

3. Results and discussion

The addition of Co to the PSSs and the RF polymerization steps led to the synthesis of the 10%Co/PSS coated materials as previously reported.[53,54] The synthesized RF coated template was then heated to decompose the PSS template and carbonization took place to form the 10%Co@HCS*x* (*x* = 16, 28, 51) materials with the three different shell thicknesses (16 nm, 28 nm, 51 nm). The methodology used was similar to that described by Li *et al.* using silica spheres as the template and RF as the carbon source.[53] The materials were characterised by classical procedures and the physical properties of the catalysts are discussed below.

Two types of catalysts were used in the reduction study, using identical reaction conditions to reduce the Co with H_2. Firstly, Co@HCS*x* catalysts were studied to obtain information on the reduction of Co by the carbon support and the H_2 as a function of shell width. Secondly, Os was added to the outside of the Co@HCS*x* catalysts to determine the effect of the Os on the Co reducibility.[21]

Table 1 Synthesis parameters used to make the HCSs with different shell thicknesses

Sample	PSS (g)	NH_3 (ml)	C_2H_5OH (ml)	H_2O (ml)	CTAB (g)	Resorcinol (g)	Formaldehyde (ml)
Co@HCS16	3	12	150	76	2	0.5	1.2
Co@HCS28	3	12	150	76	2.5	1.1	2.3
Co@HCS51	3	12	150	76	3	2.2	4.6

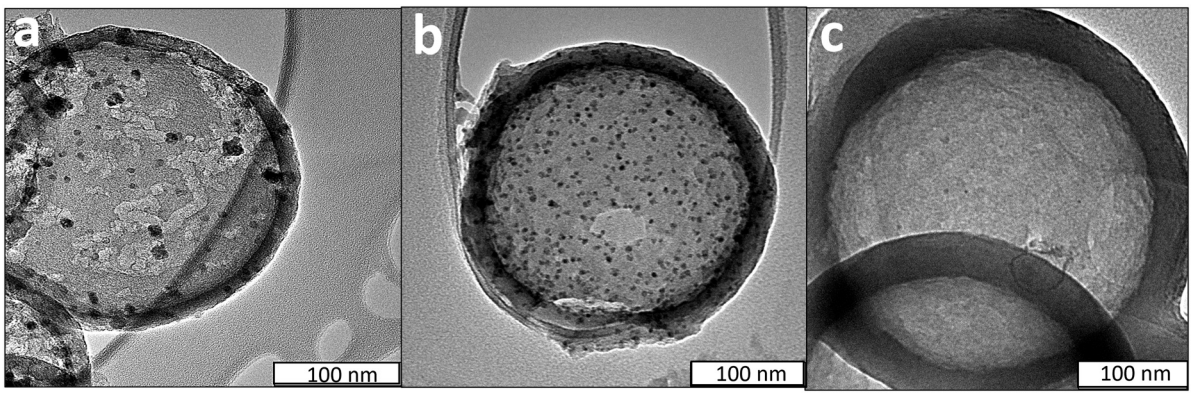

Fig. 4 TEM images of (a) 10%Co@HCS16, (b) 10%Co@HCS28 and (c) 10%Co@HCS51 catalysts (scale bar = 100 nm).

3.1 Transmission electron microscopy (TEM)

TEM images of the Co nanoparticles encapsulated inside the HCS, with different carbon shell thicknesses, are shown in Fig. 4. The HCS diameter ranged between 400 and 500 nm with the average diameter size of 448 nm (Table 2). The size of the HCSs was shown to be less than that of the PSS template and this is due to a shrinkage occurring during the carbonization process,[55] that is attributed to the dehydration of the cross-linked carbon precursor that occurs during carbonization.[56,57]

The carbon shell thickness was 16 ± 3 nm, 28 ± 5 nm, and 51 ± 6 nm for the 10%Co@HCS16, 10%Co@HCS28 and 10%Co@HCS51 catalysts, respectively. The Co nanoparticles were well dispersed and successfully encapsulated inside the HCS support. The Co nanoparticle size distribution was 7 ± 3 nm, 4 ± 1 nm, and 3.6 ± 2 for the 10%Co@HCS16, 10%Co@HCS28 and 10%Co@HCS51 catalysts, respectively (Table 2).

Fig. 5 shows the TEM images of three synthesized catalysts after Os promoter addition. The Co nanoparticles size distribution was 10 ± 8 nm, 6 ± 3 nm, and 3.7 ± 2 for the 1%Os/(10%Co@HCS16), 1%Os/(10%Co@HCS28) and 1%Os/(10%Co@HCS51) catalysts, respectively (Table 2). This data was obtained from HRTEM measurements and images at the higher resolution are shown in Fig. S6.† The Os nanoparticle size distribution was estimated by measuring the metal particles outside the HCSs and was found to be 11 ± 4 nm on average for the three catalysts (see Fig. S7†). The introduction of Os on the outer shell resulted in a small increase in the Co particle size; a similar trend was previously observed.[21]

The presence of the Co and Os were established by EDX measurements (Fig. S8 and S9†). An issue that arises relates to the actual location of the Os and Co particles. That the Co is inside the HCS can be seen from TEM tilting experiments (Fig. S7a†). The location of the Os is inferred from the synthesis method used and the lack of metal particles observed on the outside of HCSs when Os is absent from the synthesis.

3.2 Thermogravimetric analysis

Thermogravimetric analysis (TGA) was performed to i) confirm the relative Co content and ii) study the thermal stability and efficacy of template removal of the prepared samples from the carbon support, Fig. 6. The analysis was done under air and the carbon support underwent decomposition through an oxidation reaction producing CO_2 as a byproduct.

The percentage weight loss of the synthesized catalysts was compared relative to the amount of Co metal loaded, as a function of temperature as shown in Fig. 6(a) and (b). The remaining residue for the Co@HCS*x* and Os/Co@HCS*x* catalysts was attributed to the Co oxide particles, allowing an estimation of the Co metal loading percentage (~10%) inside the HCS support. Since small amounts of Os (*ca.* 1%) were loaded on the outer carbon shell, no significant difference in overall weight percentage loading was observed for the Os/Co@HCS*x* catalysts in comparison to that of Co@HCS*x* catalysts. Another possible reason for the lack of observation of an Os loading can be attributed to Os being known to undergo oxidation at 350 °C to form OsO_4 under oxidative

Table 2 Average particle size of the synthesized catalysts and their shell diameter and thickness

Sample	TEM Co particle size (nm)	TEM HCS diameter (nm)	TEM HCS shell thickness (nm)
10%Co@HCS16	7	470	16
10%Co@HCS28	4	457	28
10%Co@HCS51	5	466	51
1%Os/(10%Co@HCS16)	10	426	16
1%Os/(10%Co@HCS28)	6	468	28
1%Os/(10%Co@HCS51)	5	465	51

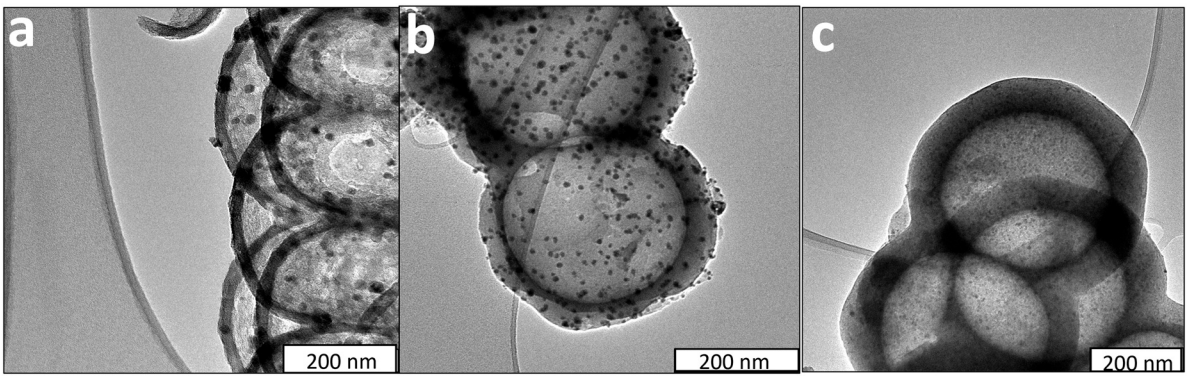

Fig. 5 TEM images of (a) 1%Os/10%Co@HCS16, (b) 1%Os/10%Co@HCS28 and (c) 1%Os/10%Co@HCS51 catalysts (scale bar = 200 nm).

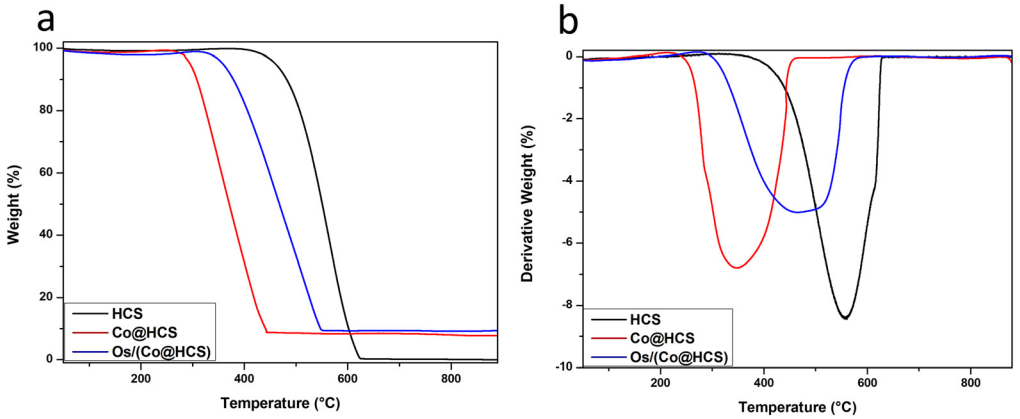

Fig. 6 (a) TGA profiles and (b) TGA first derivative plots of the HCS, Co@HCS and Os/Co@HCS.

conditions.[58] OsO_4 is volatile and is thus removed from the TGA under the experimental conditions.

The first derivate of the TGA profile for the bulk assembled synthesized catalyst curves allowed the analysis for the determination of the temperature at which the maximum weight loss took place. Thermal decomposition profiles of the catalysts are shown in Fig. S1.†

3.3 Nitrogen absorption–desorption analysis (BET)

Table 3 shows a summary of the nitrogen absorption–desorption analysis data used to determine the surface area, pore volume and pore size characteristics of the prepared catalysts. The prepared catalysts show type I/IV isotherms which is due to the presence of a carbon framework that is both mesoporous and microporous (Fig. S2†).

All of the synthesized catalysts were shown to have large BET surface areas (349–491 $m^2\ g^{-1}$). In particular, the surface areas of the Co@HCS catalysts were 392 $m^2\ g^{-1}$, 468 $m^2\ g^{-1}$, and 491 $m^2\ g^{-1}$ for the 10%Co@HCS16, 10%Co@HCS28 and 10%Co@HCS51 catalysts, respectively and thus showed an increase with shell thickness. This would be consistent with the thicker shell which provides added surface area from the carbon support. The average pore size of the catalysts was 8.7 nm, 7.3 nm, and 4.3 nm for the 10%Co@HCS16, 10%Co@HCS28 and 10%Co@HCS51 catalysts, respectively.

The promoted catalysts had surface areas of 418 $m^2\ g^{-1}$, 415 $m^2\ g^{-1}$, and 389 $m^2\ g^{-1}$ for the 1%Os(10%Co@HCS16), 1%Os(10%Co@HCS28) and 1%Os(10%Co@HCS51) catalysts, respectively and showed a decrease with shell thickness. It is assumed that pore blockage by Os as well as increase in shell thickness played a role in this observation. The pore sizes of the promoted catalysts were 9.8 nm, 8.1 nm, and 6.7 nm for the 1%Os/(10%Co@HCS16), 1%Os/(10%Co@HCS28) and 1%Os/(10%Co@HCS51) catalysts, respectively, consistent with the decreased surface areas with Os loading. The formation of catalysts with mesopore size less than 2 nm, Fig. S3,† can be attributed to the decomposition of RF and loss of small molecules during carbonization of the HCSs.[59]

3.4 Powder X-ray diffraction (PXRD)

Powder X-ray diffraction (PXRD) data were collected on the prepared catalysts for the purpose of studying the influence of the carbon shell on the crystalline phases that are present in the samples, Fig. 7. A summary of the PXRD data is given in Table S1.† All of the PXRD patterns contained a broad feature *ca.* 22.5° 2θ which is attributed to the disordered sp^2 hybridized carbon (002) reflection.[60] No notable diffraction peaks belonging to the Os phase were observed in any of the PXRD patterns due to the low promoter metal loadings.

The Co@HCS*x* (*x* = 16, 28 and 51) catalysts showed peaks belonging to the cubic Co_3O_4 phase and cubic CoO metal phase corresponding with the **COD: 1526734** and **COD: 1533087** reference patterns, respectively, Fig. 7(a). The contact between Co_3O_4 and the HCSs resulted in the formation of the CoO phase observed due to an auto-reduction process. Further, for the Co@HCS*x* (*x* = 16, 28 and 51) catalysts, the Co_3O_4 phase showed particles that were in a nanoscale range, as well as having a narrow size distribution.[61]

Table 3 Summary of the N_2 physisorption data

Sample	Surface area ($m^2\ g^{-1}$)	Pore volume ($cm^3\ g^{-1}$)	Pore size (nm)	Micropore volume ($cm^3\ g^{-1}$)
10%Co@HCS16	392	0.44	8.7	0.16
10%Co@HCS28	468	0.32	7.3	0.18
10%Co@HCS51	491	0.12	4.3	0.20
1%Os/(10%Co@HCS16)	418	0.83	9.8	0.08
1%Os/(10%Co@HCS28)	415	0.70	8.1	0.12
1%Os/(10%Co@HCS51)	389	0.53	6.7	0.15

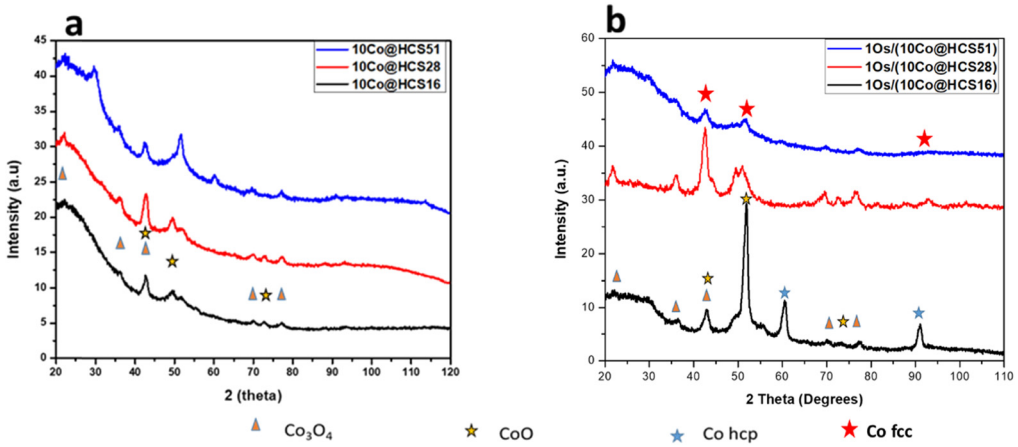

Fig. 7 PXRD patterns of (a) Co@HCS*x* (*x* = 16 nm, 28 nm, and 51 nm) and (b) Os/(Co@HCS*x*) (*x* = 16 nm, 28 nm, and 51 nm).

Similar peaks were observed after addition of the Os promoter to the outer shell of the Co@HCS*x* catalysts with the further detection of the metallic Co (fcc) phase (**COD: 9008466**), Fig. 7(b). The Co (fcc) phase was present in the Os promoted catalysts and the phase decreased with an increase in shell thickness. The reduction in the presence of Os occurs due to spillover.[62] This observation indicates that reduction of the Co oxides to Co metal by Os promoter was impeded by an increase in carbon shell thickness. This suggests that the presence of Os on the outer shell had less impact on the phase of the Co encapsulated inside the HCS support as the carbon shell thickness increased. The PXRD pattern of the Os/(Co@HCS16) catalyst, surprisingly, had strong peaks that were assigned to CoO and the hcp Co phase (**COD: 9008492**).

Overall, the information obtained from the PXRD data suggested that the intimacy of the Os promoter with the Co catalyst in the thinner carbon shell materials (Os/(Co@HCS16)) and (Os/(Co@HCS28)) catalysts promoted the reduction of CoO_x to give the hcp and fcc metallic Co phases. In contrast, when the Os promoter and Co were separated by a thicker carbon shell (Os/(Co@HCS51)), no metallic Co phases were observed.

3.5 Temperature programmed reduction (TPR)

TPR profiles of the Co@HCS*x* catalysts with different carbon shell thickness are shown in Fig. 8–10, and the data are given in Table 4. The TPR profiles of all the catalysts >450 °C showed a peak that corresponds to the methanation of the carbon support (Fig. S4 and S5†). The TPR profiles, in Fig. 8, of the different Co@HCS*x* catalysts showed two peaks as expected for the two stage reduction of Co (Co_3O_4 → CoO → Co). The first reduction event (Co_3O_4 → CoO) showed that an increase in carbon shell thickness resulted in a higher reduction temperature for the Co oxide. This effect must be due to H_2 diffusion. The second reduction peak (CoO → Co) had very similar peak positions and little change with carbon shell thickness suggesting no/less diffusion effects.

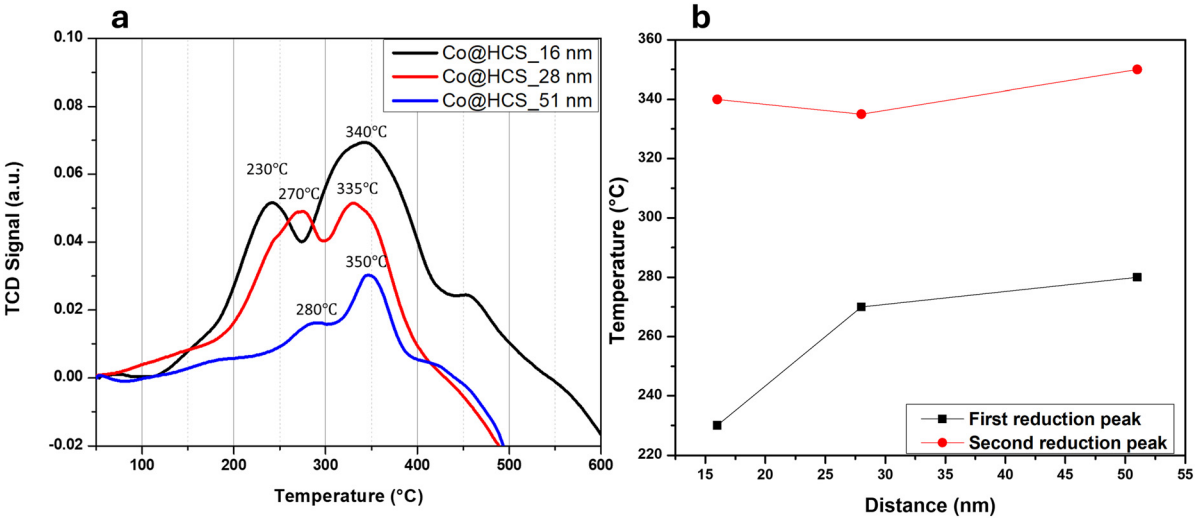

Fig. 8 TPR profiles of (a) Co@HCS16, Co@HCS28 and Co@HCS5, and (b) reduction temperature *versus* HCS diameter (distance).

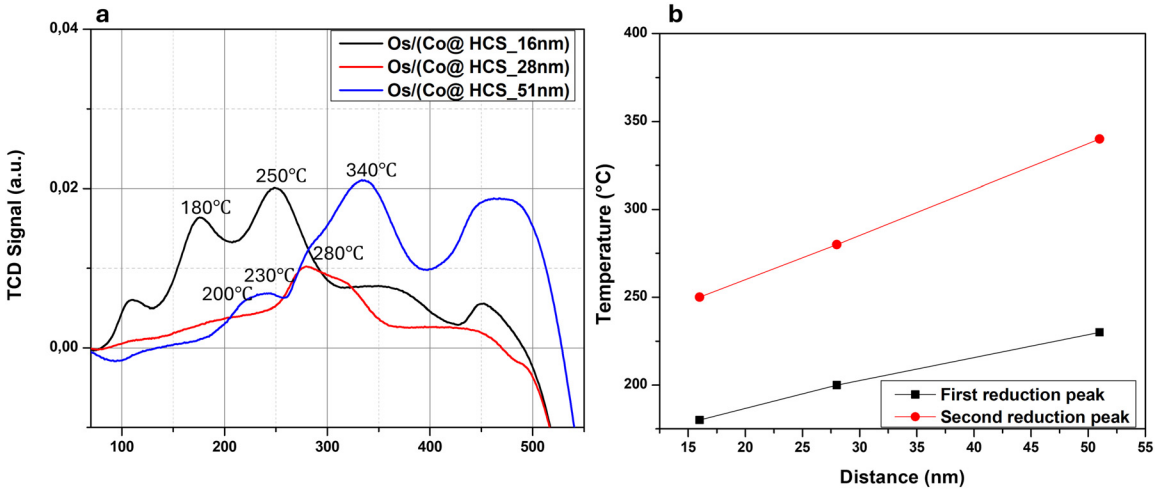

Fig. 9 TPR profiles of (a) Os/(Co@HCS16), Os/(Co@HCS28) and Os/(Co@HCS51), and (b) reduction temperature *versus* HCS diameter (distance).

The TPR profiles of Os/(Co@HCS*x*) catalysts with different carbon shell thickness are shown in Fig. 9(a). The Os/(10%Co@HCS*x*) (x = 16 nm, and 51 nm) catalysts showed a peak at temperatures below 120 °C and this peak can be attributed to the evolution of water. Fig. 9(b) shows the effect of variation of the carbon shell thickness on the TPR peaks for the Co reduction. Also shown are the data for OsCo@HCS28 (ref. 21) and Co@HCS*x* (x = 16, 28, 51), Fig. 10. This data shows Co in contact with Os (d = 0) and Co not in contact with Os, respectively. The TPR profiles of the catalysts revealed that a change in shell thickness between the Os promoter and Co_3O_4 catalyst decreased the reducibility of both Co reduction steps. These peak position changes could be due to i) pore size and diffusion (physical) effects, ii) effects associated with the cobalt oxides or iii) distance (spillover) effects.

TPR first reduction peaks. The increase in carbon shell thickness of the Os/(Co@HCS*x*) catalyst resulted in a decrease of the reduction temperature relative to the Co@HCS*x* catalysts. The plot shows a similar slope for both catalysts suggesting that both diffusion and spillover are occurring. The data are consistent with Os 'acting at a distance' with the Co reduction dependent on the shell thickness.

TPR second reduction peaks. Again, as the thickness increased the peak position shifted to higher temperatures. Since the data can be compared with the Os@HCS data, this effect must be due to spillover effects and not diffusion effects. The possibility of effects due to the various degrees of Co reduction prior to the TPR study could also influence the actual peak positions. Indeed the 10%Co@HCS51 nm catalyst was shown to have Co in the CoO phase due to carbon auto-reduction.[63] Also, it is recognised that the peak positions will be affected by the different pore size data.

A related study of distance variation between two metals was conducted using Fe oxide and a Pt promoter.[8] X-ray absorption spectroscopy (XAS) measurements revealed the Fe degree of reduction as a function of distance (0 to 45 nm) from a Pt particle.[64–66] When supported on a nonreducible aluminium oxide support the reduction of Fe oxide decreased (to zero) with an increase in distance. Our study allowed us to evaluate the effect of a carbon support on the spillover effect. As can be seen from Fig. 10 it appears that the Os–Co separation effects the two step reduction differently. The second reduction step appears to have a maximum distance

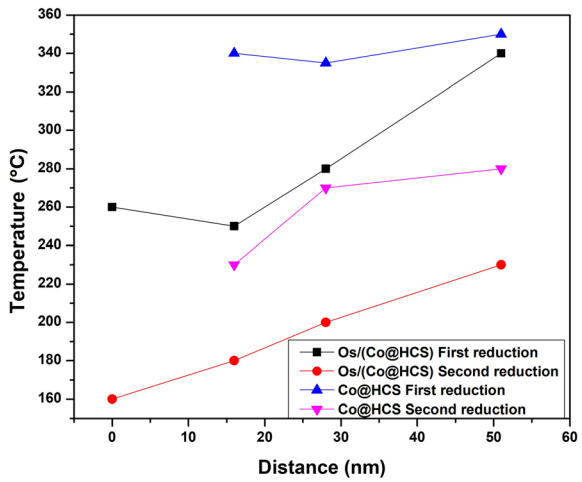

Fig. 10 Effect of distance (shell thickness) on the reduction peaks of Os/Co@HCS*x* (x = 10, 28, 51), OsCo@HCS_28 nm (peak at distance 0 nm (ref. 21)) and Co@HCS (x = 16, 28, 51).

Table 4 Summary of the TPR first and second reduction data

Sample	First reduction (°C)	Second reduction (°C)
10%Co@HCS16	230	340
10%Co@HCS28	260	335
10%Co@HCS51	280	350
1%Os10%Co@HCS28 (ref. 21)	160	260
1%Os/(10%Co@HCS16)	180	250
1%Os/(10%Co@HCS28)	200	280
1%Os/(10%Co@HCS51)	230	340

of *ca.* 50 nm for complete reduction whereas the first reduction step, by extrapolation of the data in Fig. 9 appears to have a maximum distance of about 100 nm.

It is known that metal reducibility is affected by other factors that include particle size and the crystalline phase of the Co species. The particle sizes of the Os are constant while the Co size did show some variation which would impact on the FTS data but should have only a small effect on the TPR data. It is also noted that the Co phases are impacted by the thickness of the carbon layer, most probably linked to different degrees of reduction by the amount of carbon available. However, this should not have a large impact on the TPR peak positions, but will have an effect on the relative peak sizes associated with the Co species present. This indeed is observed.

The mechanism by which the spillover has occurred has not as yet been explored in this study. However carbon spheres (CSs) with graphitic flakes' edges make excellent sites for hydrogen absorption and also the reduction of CoO to metallic Co.[67,68] This suggests that the spillover on the HCSs is influenced by the defects on the carbon as proposed by others.[52,69] Thus, the degree of H spillover can also be modified by variation of the defect concentration and doping type.

3.6 Fischer–Tropsch synthesis (FTS)

The FTS activity was determined in a fixed-bed micro-reactor at 220 and 250 °C (50 h at each reaction temperature) after the catalysts had been reduced at 350 °C. A summary of the catalytic performance and selectivity obtained is given in Table 5.

The Co nanoparticles with no Os, encapsulated inside the HCSs (10%Co@HCS28), was used as a standard to investigate the FTS performance. This was used to compare the effect of the carbon shell thickness on the Os promoter loaded onto the outside of the HCS. The activity of all the promoted catalysts was, as expected, higher compared to the unpromoted catalysts (Table 4). The CO conversion increased in the following order: Os/(Co@HCS51) < Os/(Co@HCS28) < Os/(Co@HCS16). This effect can be explained by factors such as the reactant and product diffusion effects, the particle size and the phase of metallic Co nanoparticles, and the permeability of the HCSs. A similar trend was observed in the TPR studies where a decrease in permeability with an increase in the carbon shell thickness resulted in a lowered amount of reduction of the Co_3O_4 into Co^0 metal. An increase in reaction temperature gave the expected increase in activity.

In FTS the Co catalyst is selective towards the production of high molecular products ($>C_{5+}$).[70] As expected, the FTS data showed that Os promoted Co@HCS catalysts resulted in higher molecular products being favoured relative to the Os free catalyst (Table 5), and an increase in methane selectivity with FTS temperature. While the data do show varying activities it appears that as the HCS thickness increased so did the C_{5+} content (at both temperatures). This could suggest that a thicker carbon shell, Co@HCS51, can inhibit the flow of products, leading to long chain growth within the HCS, resulting in the higher selectivity towards C_{5+} hydrocarbon being produced. Thus, the Co selectivity will be determined by maintaining the Co in a reduced state (thin shell), but with formation of long chain FT products (thick shell).

The data thus suggest that there is no advantage on the use of HCSs with shells that are too thick in FTS, even though spillover can occur over the distances studied. There will thus be an optimum distance between a promoter and a support to control the diffusion of products/reactants and enhance the reducibility/activity of Co on carbon supports, to lead to optimum FT selectivity/activity.

4. Conclusions

In this study, Co nanoparticles were successfully synthesized and encapsulated inside a carbon shell support (HCS) with varying thicknesses. The TPR studies showed that as the carbon shell thickness decreased, the reducibility of Co_3O_4 to metallic Co occurred in the following order: Co@HCS16 < Co@HCS28 < Co@HCS51. H_2 diffusion through the carbon shell impacted on the Co reduction. The catalysts were then promoted with Os on the outside of the HCS to investigate any secondary hydrogen spillover effects. In all three cases the reducibility of Co_3O_4 was found to be enhanced by the addition of an Os promoter suggesting that reduction occurred by H spillover in preference to H_2 diffusion leading to direct Co_3O_4 reduction. Significant shifts of the TPR peaks of the Co were observed with decreasing carbon thickness. Importantly spillover was observed at distance of >100 nm (Co_3O_4 to CoO) and to *ca.* 50 nm (CoO to Co) for the two

Table 5 A summary of the Fischer–Tropsch catalytic performance and selectivity

Sample name	Reaction temperature	CO conversion (%)	Selectivity (C mol) (%)		
			C_1	C_2–C_4	C_{5+}
10%Co@HCS28	220	4.2	18.8	11.1	70.1
	250	9.8	20.5	13.2	66.3
1%Os/(10%Co@HCS16)	220	7.4	12.3	3.9	83.8
	250	18.0	16.6	5.8	77.6
1%Os/(10%Co@HCS28)	220	5.0	13.0	3.4	83.6
	250	9.5	17.7	4.4	77.8
1%Os/(10%Co@HCS51)	220	1.6	5.1	3.1	91.2
	250	2.8	8.2	4.2	87.5

processes. Thus, spillover on carbon can occur over significant distances, presumably due to the defective carbon support. More importantly it appears that spillover varies with the ease of the metal oxide reduction potentials and that the carbon support allows for the separation of this effect.

A higher FT CO conversion was associated with the thin carbon shell catalyst Co@HCS16 indicating that diffusion effects impacted on the FT catalyst activity. The incorporation of the Os promoter improved the CO conversion and shifted the selectivity towards the production of longer chain hydrocarbons. This trend suggests that a thicker carbon shell, *e.g.* in Co@HCS51, inhibits the flow of reactants, leading to lower CO conversions and long chain products forming within the HCS, thus resulting in a higher selectivity towards C_{5+} hydrocarbon being produced. Thus, by careful choice of a thin but strong HCS shell with good porosity, maximization of Co reducibility by auto reduction and spillover effects should give a catalyst with the best activity while also producing long chain hydrocarbons.

Data availability

Data were mainly generated during the PhD study of Dr Tshepo Molefe. The thesis can be accessed at the University of the Witwatersrand. It is freely available. ESI† is included with this submission. Any queries and requests for data can be sent to the authors. All work from others has been referenced.

Author contributions

The manuscript was written through the contributions of all authors. All authors have approved the final version of the manuscript.

Conflicts of interest

We wish to confirm that there are no known conflicts of interest associated with this publication. All the sources of funding for the work described in this publication are acknowledged in the article to be published. We confirm that the manuscript has been read and approved by all named authors. We confirm that the order of authors listed in the manuscript has been approved by all named authors.

Acknowledgements

We wish to thank the University of Witwatersrand, the NRF and the DSI-NRF Centre of Excellence in Catalysis for financial support.

References

1 G.-C. Zhao, Y.-Q. Qiu and C.-G. Liu, *Appl. Catal., A*, 2021, **610**, 117948.
2 H. Shen, H. Li, Z. Yang and C. Li, *Green Energy Environ.*, 2022, **7**, 1161–1198.
3 A. Anson, E. Lafuente, E. Urriolabeitia, R. Navarro, A. M. Benito, W. K. Maser and M. T. Martínez, *J. Phys. Chem. B*, 2006, **110**, 6643–6648.
4 A. E. Aksoylu, M. Madalena, A. Freitas, M. F. R. Pereira and J. L. Figueiredo, *Carbon*, 2001, **39**, 175–185.
5 C. Amorim and M. A. Keane, *J. Colloid Interface Sci.*, 2008, **322**, 196–208.
6 S.-J. Park and S.-Y. Lee, *Int. J. Hydrogen Energy*, 2010, **35**, 13048–13054.
7 S. Khoobiar, *J. Phys. Chem.*, 1964, **68**, 411–412.
8 W. Karim, C. Spreafico, A. Kleibert, J. Gobrecht, J. VandeVondele, Y. Ekinci and J. A. van Bokhoven, *Nature*, 2017, **541**, 68–71.
9 A. J. Lachawiec, G. Qi and R. T. Yang, *Langmuir*, 2005, **21**, 11418–11424.
10 S. J. Teichner, in *Studies in Surface Science and Catalysis*, Elsevier, 1993, vol. 77, pp. 27–43.
11 A. Lueking and R. T. Yang, *J. Catal.*, 2002, **206**, 165–168.
12 M. Hirscher and M. Becher, *J. Nanosci. Nanotechnol.*, 2003, **3**, 3–17.
13 Y.-Y. Liu, J.-L. Zeng, J. Zhang, F. Xu and L.-X. Sun, *Int. J. Hydrogen Energy*, 2007, **32**, 4005–4010.
14 R. Prins, *Chem. Rev.*, 2012, **112**, 2714–2738.
15 C. Scarfiello, A. Durupt, Y. Tison, D. Pham Minh, K. Soulantica and P. Serp, *Catal. Sci. Technol.*, 2024, **14**, 2896–2907.
16 D. Nabaho, J. W. H. Niemantsverdriet, M. Claeys and E. Van Steen, *Catal. Today*, 2016, **261**, 17–27.
17 M. Choi, S. Yook and H. Kim, *ChemCatChem*, 2015, **7**, 1048–1057.
18 M. Tang, P. E. de Jongh and K. P. de Jong, *Small*, 2024, **20**, 2304683.
19 J. Wei, S. Qin, J. Liu, X. Ruan, Z. Guan, H. Yan, D. Wei, H. Zhang, J. Cheng and H. Xu, *Angew. Chem., Int. Ed.*, 2020, **59**, 10343–10347.
20 Z. Hu, T. Zhang, D. Li and R. T. Yang, *Catal. Sci. Technol.*, 2021, **11**, 886–894.
21 T. Molefe, D. Barrett, B. Diaz, R. Forbes and N. J. Coville, *J. Catal.*, 2023, **424**, 246–257.
22 P. Jain, D. A. Fonseca, E. Schaible and A. D. Lueking, *J. Phys. Chem. C*, 2007, **111**, 1788–1800.
23 D. Lupu, A. R. Biriș, I. Mișan, A. Jianu, G. Holzhüter and E. Burkel, *Int. J. Hydrogen Energy*, 2004, **29**, 97–102.
24 C.-K. Back, G. Sandí, J. Prakash and J. Hranisavljevic, *J. Phys. Chem. B*, 2006, **110**, 16225–16231.
25 E. Yoo, L. Gao, T. Komatsu, N. Yagai, K. Arai, T. Yamazaki, K. Matsuishi, T. Matsumoto and J. Nakamura, *J. Phys. Chem. B*, 2004, **108**, 18903–18907.
26 R. Zacharia, K. Y. Kim, A. K. M. F. Kibria and K. S. Nahm, *Chem. Phys. Lett.*, 2005, **412**, 369–375.
27 C.-H. Chen and C.-C. Huang, *Microporous Mesoporous Mater.*, 2008, **109**, 549–559.
28 Y. Suttisawat, P. Rangsunvigit, B. Kitiyanan, M. Williams, P. Ndungu, M. V. Lototskyy, A. Nechaev, V. Linkov and S. Kulprathipanja, *Int. J. Hydrogen Energy*, 2009, **34**, 6669–6675.

29 R. Bhowmick, S. Rajasekaran, D. Friebel, C. Beasley, L. Jiao, H. Ogasawara, H. Dai, B. Clemens and A. Nilsson, *J. Am. Chem. Soc.*, 2011, **133**, 5580–5586.
30 R. Zacharia, S. Rather, S. W. Hwang and K. S. Nahm, *Chem. Phys. Lett.*, 2007, **434**, 286–291.
31 A. Reyhani, S. Z. Mortazavi, S. Mirershadi, A. Z. Moshfegh, P. Parvin and A. N. Golikand, *J. Phys. Chem. C*, 2011, **115**, 6994–7001.
32 H. Wu, D. Wexler and H. Liu, *Int. J. Hydrogen Energy*, 2012, **37**, 5686–5690.
33 D. Saha and S. Deng, *Langmuir*, 2011, **27**, 6780–6786.
34 L. Zubizarreta, J. A. Menéndez, J. J. Pis and A. Arenillas, *Int. J. Hydrogen Energy*, 2009, **34**, 3070–3076.
35 R. Campesi, F. Cuevas, R. Gadiou, E. Leroy, M. Hirscher, C. Vix-Guterl and M. Latroche, *Carbon*, 2008, **46**, 206–214.
36 C.-H. Chen, T.-Y. Chung, C.-C. Shen, M.-S. Yu, C.-S. Tsao, G.-N. Shi, C.-C. Huang, M.-D. Ger and W.-L. Lee, *Int. J. Hydrogen Energy*, 2013, **38**, 3681–3688.
37 B. P. Vinayan, K. Sethupathi and S. Ramaprabhu, *Int. J. Hydrogen Energy*, 2013, **38**, 2240–2250.
38 B. P. Vinayan, K. Sethupathi and S. Ramaprabhu, *J. Nanosci. Nanotechnol.*, 2012, **12**, 6608–6614.
39 V. B. Parambhath, R. Nagar and S. Ramaprabhu, *Langmuir*, 2012, **28**, 7826–7833.
40 D. Giasafaki, G. Charalambopoulou, A. Bourlinos, A. Stubos, D. Gournis and T. Steriotis, *Adsorption*, 2013, **19**, 803–811.
41 C. Zlotea, F. Cuevas, V. Paul-Boncour, E. Leroy, P. Dibandjo, R. Gadiou, C. Vix-Guterl and M. Latroche, *J. Am. Chem. Soc.*, 2010, **132**, 7720–7729.
42 Y.-X. Yang, L. Bourgeois, C. Zhao, D. Zhao, A. Chaffee and P. A. Webley, *Microporous Mesoporous Mater.*, 2009, **119**, 39–46.
43 J. Im, H. Shin, H. Jang, H. Kim and M. Choi, *Nat. Commun.*, 2014, **5**, 1–8.
44 K. Motokura, *Chem. – Asian J.*, 2024, e202301083.
45 F. P. Hu, Z. Wang, Y. Li, C. Li, X. Zhang and P. K. Shen, *J. Power Sources*, 2008, **177**, 61–66.
46 R. Liu, F. Qu, Y. Guo, N. Yao and R. D. Priestley, *Chem. Commun.*, 2014, **50**, 478–480.
47 V. A. De La Peña O'Shea, M. C. Álvarez-Galván, J. M. Campos-Martin, N. N. Menéndez, J. D. Tornero and J. L. G. Fierro, *Eur. J. Inorg. Chem.*, 2006, 5057–5068.
48 T. Harada, S. Ikeda, Y. H. Ng, T. Sakata, H. Mori, T. Torimoto and M. Matsumura, *Adv. Funct. Mater.*, 2008, **18**, 2190–2196.
49 M. C. Bahome, L. L. Jewell, D. Hildebrandt, D. Glasser and N. J. Coville, *Appl. Catal., A*, 2005, **287**, 60–67.
50 M.-M. Titirici, M. Antonietti and N. Baccile, *Green Chem.*, 2008, **10**, 1204–1212.
51 J. Fu, Q. Xu, J. Chen, Z. Chen, X. Huang and X. Tang, *Chem. Commun.*, 2010, **46**, 6563–6565.
52 T. N. Phaahlamohlaka, D. O. Kumi, M. W. Dlamini, R. Forbes, L. L. Jewell, D. G. Billing and N. J. Coville, *ACS Catal.*, 2017, **7**, 1568–1578.
53 N. Li, Q. Zhang, J. Liu, J. Joo, A. Lee, Y. Gan and Y. Yin, *Chem. Commun.*, 2013, **49**, 5135–5137.
54 X. Fang, S. Liu, J. Zang, C. Xu, M.-S. Zheng, Q.-F. Dong, D. Sun and N. Zheng, *Nanoscale*, 2013, **5**, 6908–6916.
55 S. Li, A. Pasc, V. Fierro and A. Celzard, *J. Mater. Chem. A*, 2016, **4**, 12686–12713.
56 M. Zheng, J. Cao, X. Chang, J. Wang, J. Liu and X. Ma, *Mater. Lett.*, 2006, **60**, 2991–2993.
57 W. Stober and A. Fink, *J. Colloid Interface Sci.*, 1968, **26**, 62–69.
58 S. E. Livingstone, *The Chemistry of Ruthenium, Rhodium, Palladium, Osmium, Iridium and Platinum: Pergamon Texts in Inorganic Chemistry*, Elsevier, 2016, vol. 25.
59 X. Ma, L. Gan, M. Liu, P. K. Tripathi, Y. Zhao, Z. Xu, D. Zhu and L. Chen, *J. Mater. Chem. A*, 2014, **2**, 8407–8415.
60 A. C. Ferrari and J. Robertson, *Phys. Rev. B: Condens. Matter Mater. Phys.*, 2000, **61**, 14095.
61 C. Weidenthaler, *Nanoscale*, 2011, **3**, 792–810.
62 T. N. Phaahlamohlaka, D. O. Kumi, M. W. Dlamini, R. Forbes, L. L. Jewell, D. G. Billing and N. J. Coville, *ACS Catal.*, 2017, **7**, 1568–1578.
63 W. Chen, X. Pan, M.-G. Willinger, D. S. Su and X. Bao, *J. Am. Chem. Soc.*, 2006, **128**, 3136–3137.
64 W. Karim, A. Kleibert, U. Hartfelder, A. Balan, J. Gobrecht, J. A. van Bokhoven and Y. Ekinci, *Sci. Rep.*, 2016, **6**, 1–8.
65 J. A. Van Bokhoven and C. Lamberti, *X-ray absorption and X-ray emission spectroscopy: theory and applications*, John Wiley & Sons, 2016, vol. 1.
66 C. A. F. Vaz, A. Balan, F. Nolting and A. Kleibert, *Phys. Chem. Chem. Phys.*, 2014, **16**, 26624–26630.
67 Z. L. Wang and Z. C. Kang, *Carbon*, 1997, **35**, 419–426.
68 Z. C. Kang and Z. L. Wang, *J. Phys. Chem.*, 1996, **100**, 5163–5165.
69 S. Ikeda, S. Ishino, T. Harada, N. Okamoto, T. Sakata, H. Mori, S. Kuwabata, T. Torimoto and M. Matsumura, *Angew. Chem., Int. Ed.*, 2006, **45**, 7063–7066.
70 G. P. Van Der Laan and A. A. C. M. Beenackers, *Catal. Rev.: Sci. Eng.*, 1999, **41**, 255–318.